Supplementary Information

Bromine Substitution Improves Excited-State Dynamics in Mesoporous Mixed Halide Perovskite Films

Eric M. Talbert,[a‡] Holly F. Zarick,[a‡] Abdelaziz Boulesbaa,[b] Naiya Soetan,[a] Alexander A. Puretzky,[b] David B. Geohegan,[b] and Rizia Bardhan[a*]

[a]Department of Chemical and Biomolecular Engineering, Vanderbilt University, Nashville, TN 37235, USA
[b]Center for Nanophase Materials Sciences, Oak Ridge National Laboratory, Oak Ridge, TN 37831, USA

‡Equal contributing first authors
*Corresponding Author: rizia.bardhan@vanderbilt.edu

Tables and Figures

Table S1. The following amounts of MAI and MABr were added to 7 mL IPA to generate the stochiometric ratios necessary for the desired Br content.

Br Content (x)	**MAI** (mg)	**MABr** (mg)
0	105	0
10	84	15
20	70	24
30	59	33

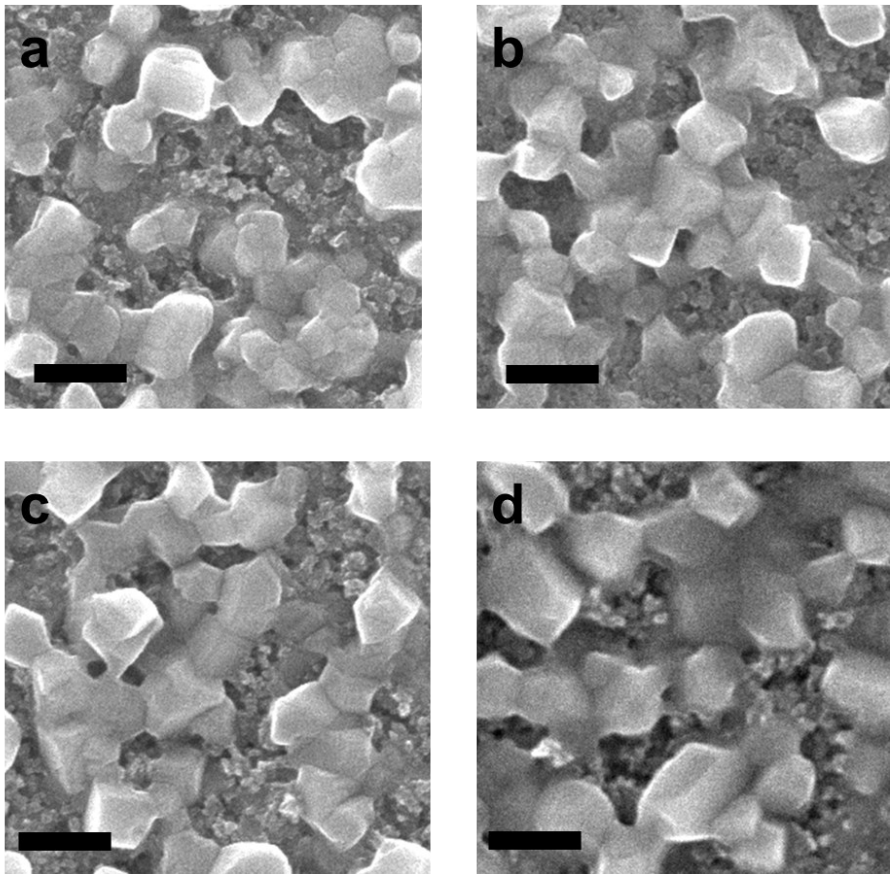

Figure S1. SEM micrographs of $CH_3NH_3Pb(I_{1-x}Br_x)_3$ show that grain morphology is consistent across Br compositions. Top views of perovskite films deposited with x = 0, 0.1, 0.2, and 0.3 are shown in (a), (b), (c), and (d), respectively. All scale bars are 200 nm.

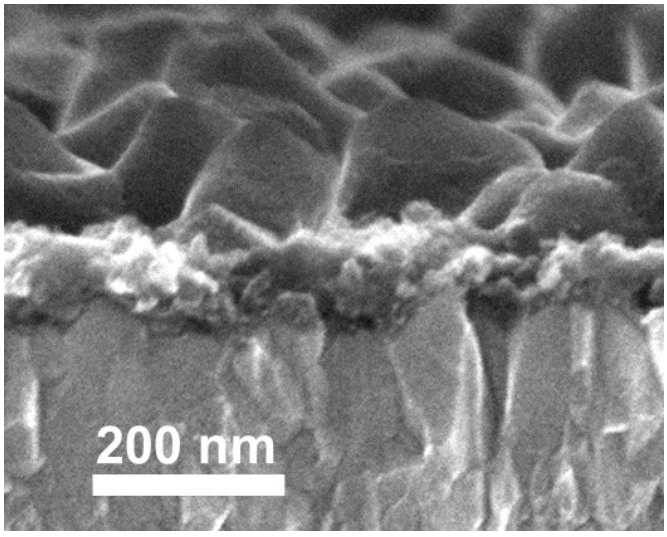

Figure S2. Non-color modified representative cross-sectional SEM of a 100 nm mesoporous-TiO_2 layer infiltrated with $MAPb(I_{1-x}Br_x)_3$, from main text Figure 1b. Shown here is x = 0 Br incorporation.

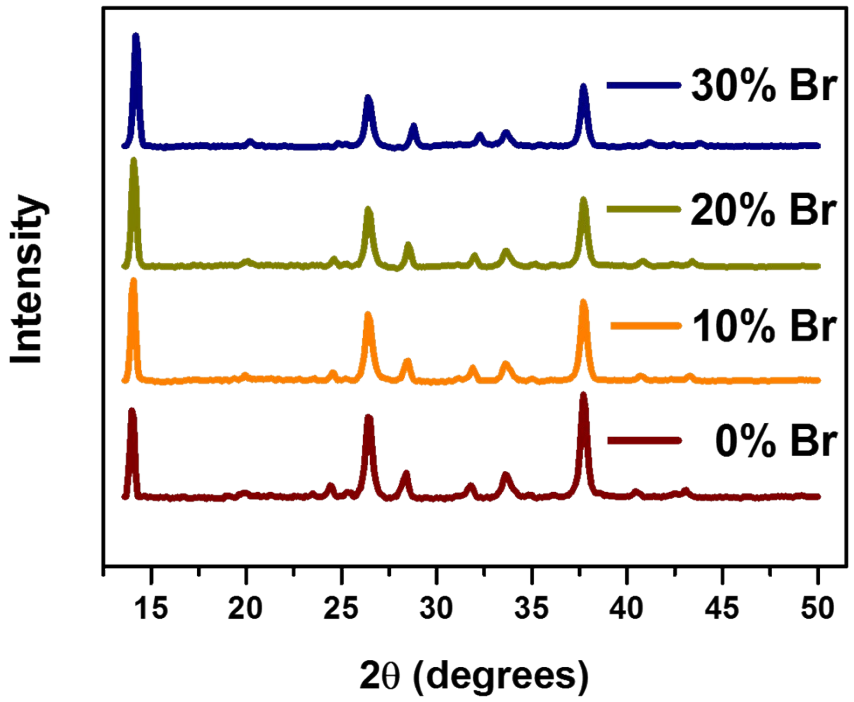

Figure S3. Full glancing angle XRD spectra for all samples, depicting the characteristic peaks of $MAPb(I_{1-x}Br_x)_3$ perovskite and anatase TiO_2.

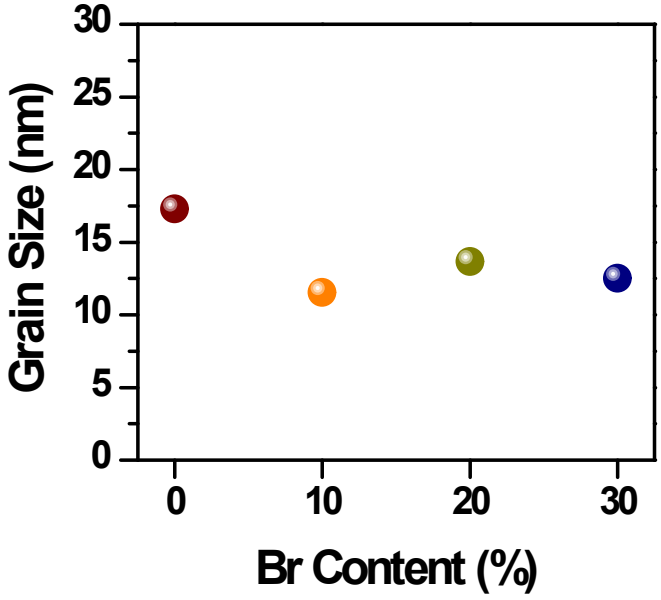

Figure S4. Average crystallite diameter calculated from the Scherrer equation. The crystallite diameter is relatively consistent across all Br compositions, especially considering that the Br-containing samples show a slight underestimate of grain size due to inherent compositional variations.

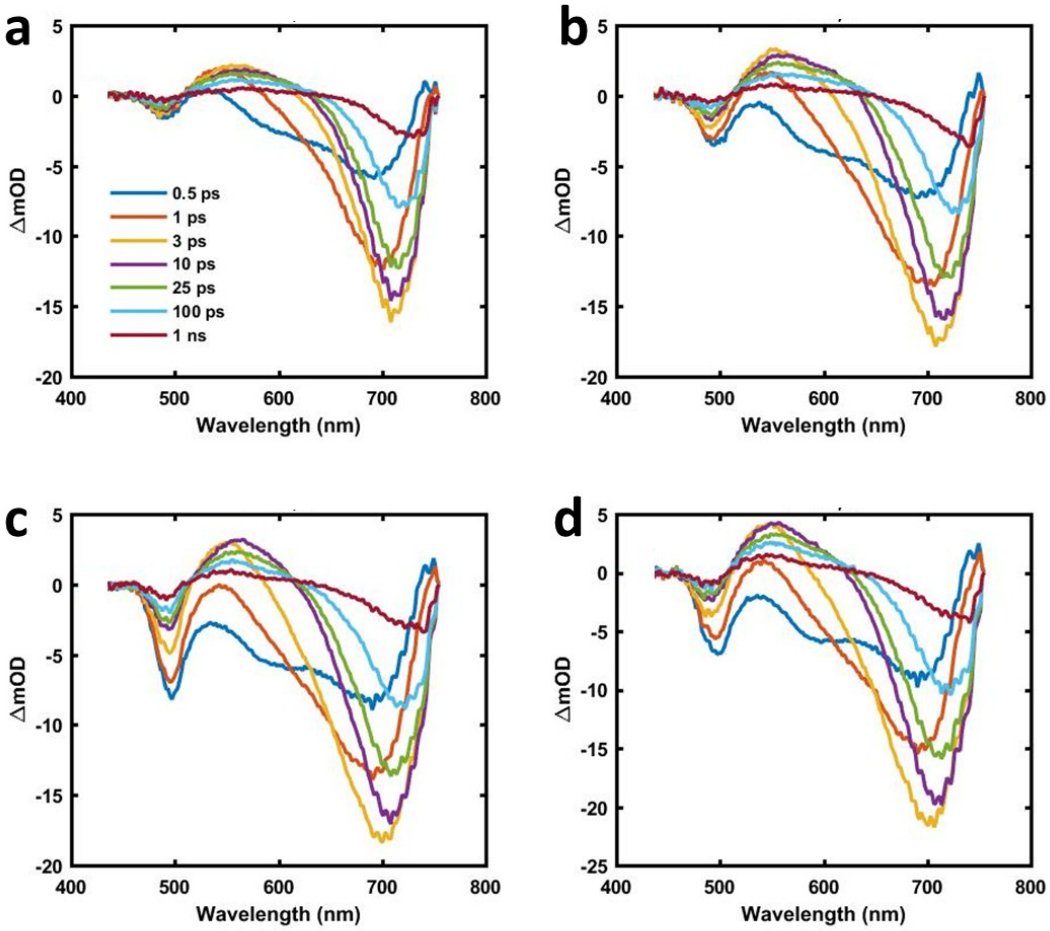

Figure S5. Transient absorption spectra at various time delays of a mesoporous TiO_2 film infiltrated with $MAPb(I_{1-x}Br_x)_3$ with x=0 at various excitation fluences, (a) 20 μJ/pulse, (b) 40 μJ/pulse, (c) 60 μJ/pulse, and (d) 80 μJ/pulse.

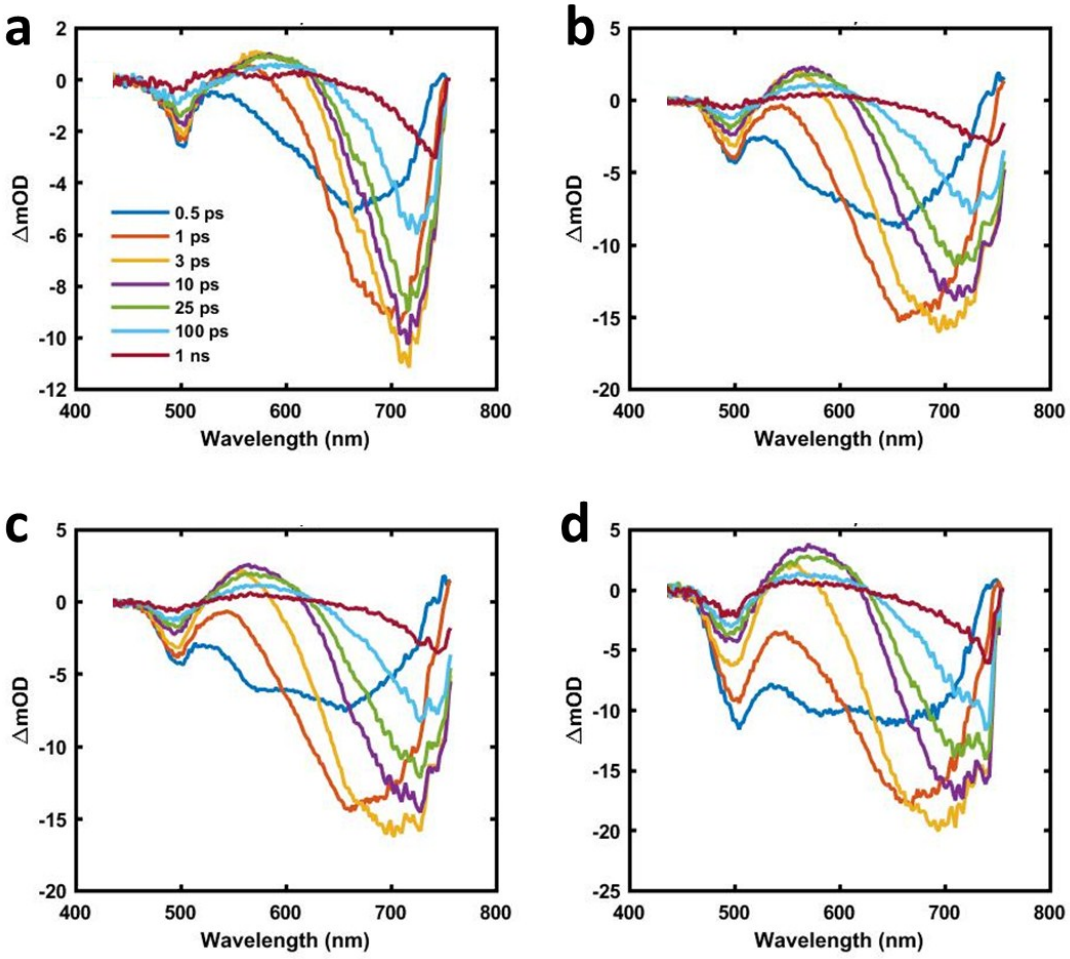

Figure S6. Transient absorption spectra at various time delays of a mesoporous TiO_2 film infiltrated with $MAPb(I_{1-x}Br_x)_3$ with x=0.1 at various excitation fluences, (a) 20 μJ/pulse, (b) 40 μJ/pulse, (c) 60 μJ/pulse, and (d) 80 μJ/pulse.

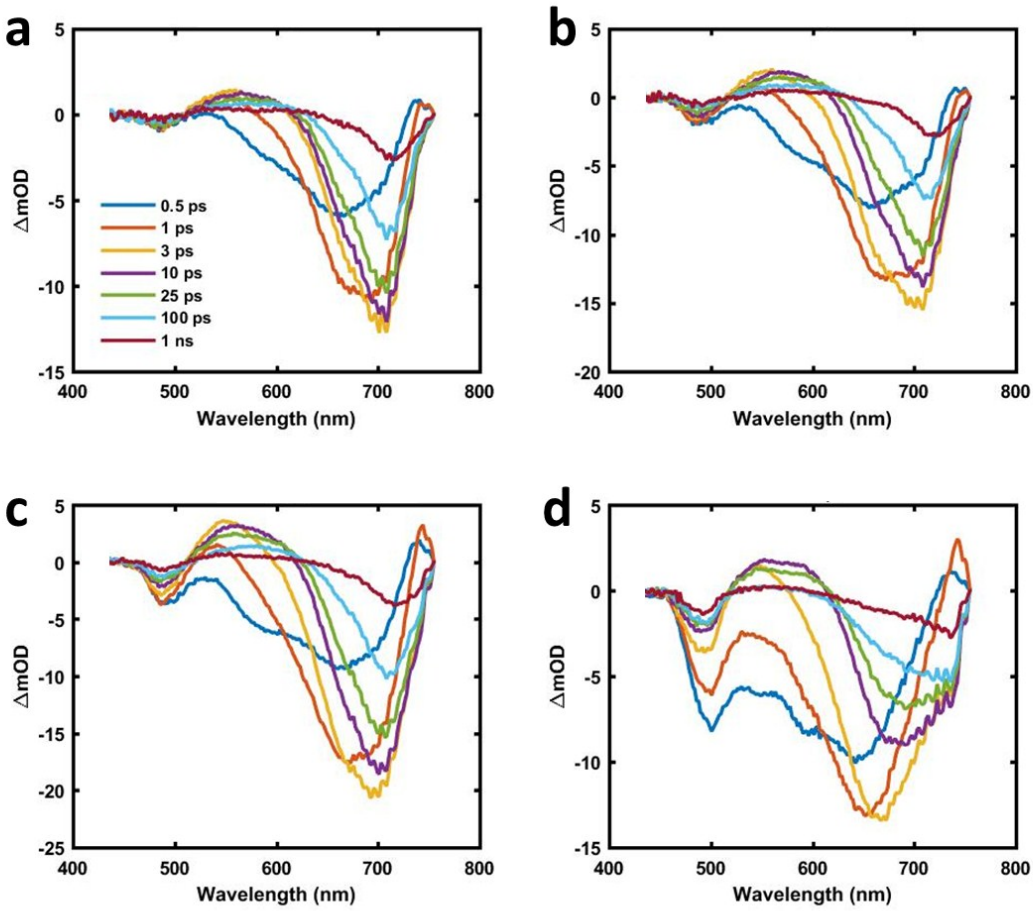

Figure S7. Transient absorption spectra at various time delays of a mesoporous TiO_2 film infiltrated with $MAPb(I_{1-x}Br_x)_3$ with x=0.2 at various excitation fluences, (a) 20 μJ/pulse, (b) 40 μJ/pulse, (c) 60 μJ/pulse, and (d) 80 μJ/pulse.

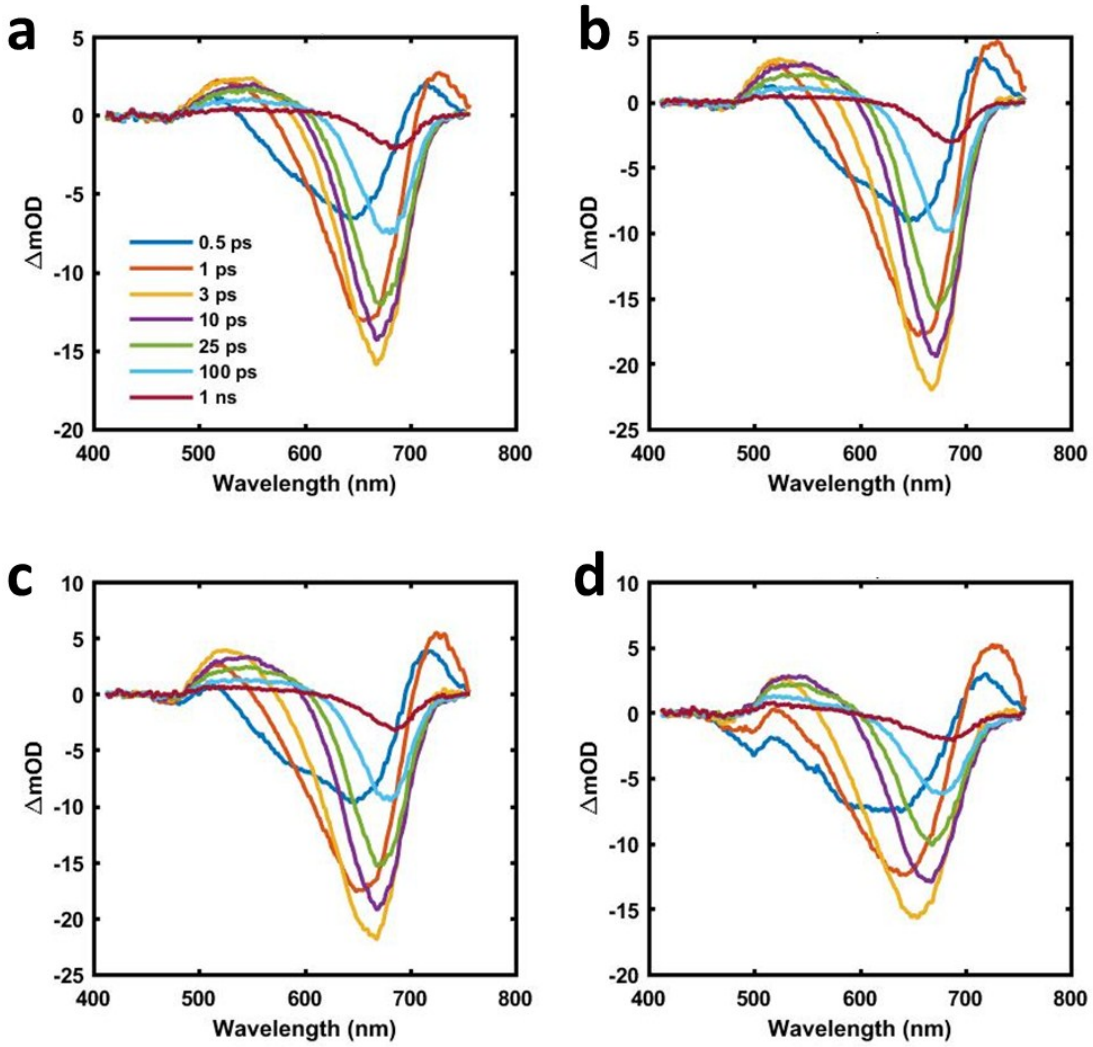

Figure S8. Transient absorption spectra at various time delays of a mesoporous TiO_2 film infiltrated with $MAPb(I_{1-x}Br_x)_3$ with x=0.3 at various excitation fluences, (a) 20 μJ/pulse, (b) 40 μJ/pulse, (c) 60 μJ/pulse, and (d) 80 μJ/pulse.

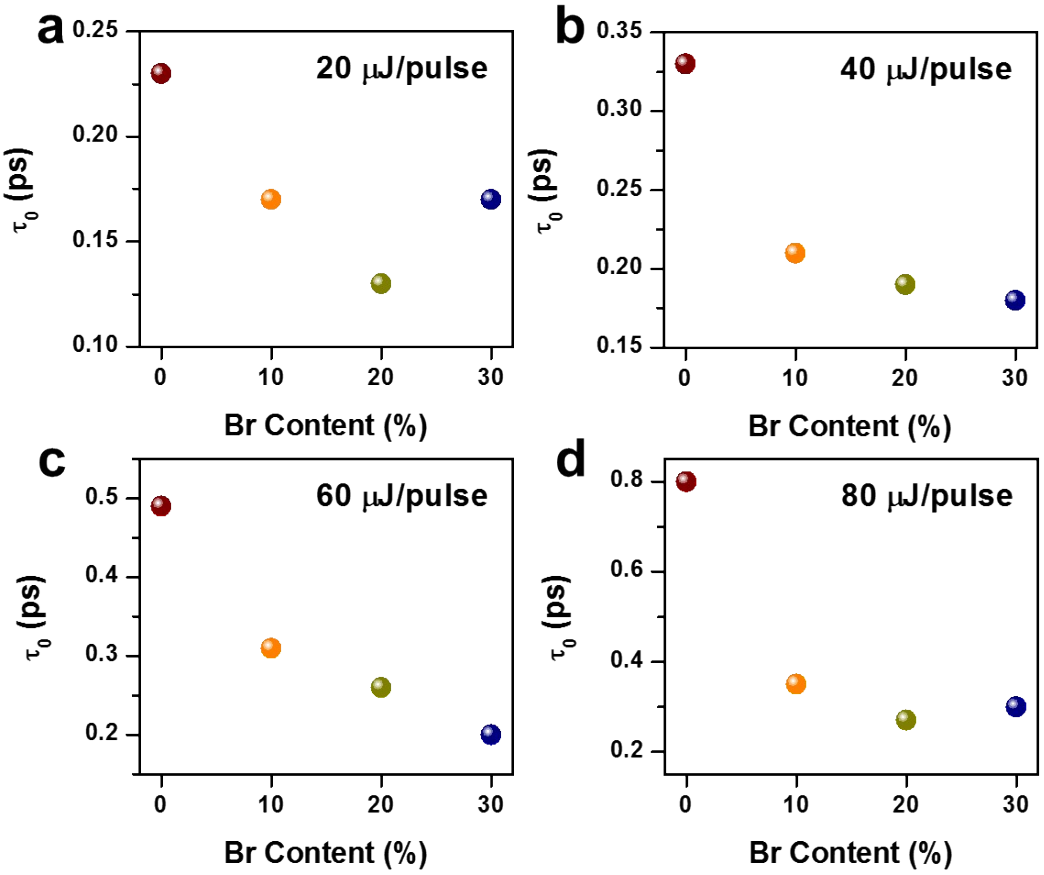

Figure S9. Calculated thermalization lifetime data (τ_0) derived from triexponential fits of transient absorption photobleach dynamics of $MAPb(I_{1-x}Br_x)_3$-infiltrated mesoporous TiO_2 films as a function of Br content and at various excitation fluences, (a) 20 μJ/pulse, (b) 40 μJ/pulse, (c) 60 μJ/pulse, and (d) 80 μJ/pulse. Corresponding amplitudes (A_0) of the normalized data were fixed to -1.

Table S2. Premature recombination lifetimes (τ_1) and charge injection lifetimes (τ_2) and corresponding amplitudes (A) derived from triexponential fits of transient absorption photobleach recoveries of $MAPb(I_{1-x}Br_x)_3$ -infiltrated mesoporous-TiO_2 films as a function of Br content and excitation energy. R squared values to check for goodness of fit are provided as well.

Br Content (%)	**Excitation Energy** (μJ/pulse)	A_1	τ_1 (ps)	A_2	τ_2 (ps)	R^2
0	20	0.52	32.6	0.36	786	0.992
	40	0.58	20.0	0.35	473	0.991
	60	0.56	15.6	0.36	378	0.982
	80	0.63	15.1	0.34	390	0.986
10	20	0.43	17.9	0.39	574	0.984
	40	0.55	12.6	0.36	421	0.987
	60	0.65	15.4	0.37	416	0.994
	80	0.66	13.8	0.36	755	0.992
20	20	0.47	27.4	0.43	536	0.992
	40	0.55	21.4	0.36	457	0.986
	60	0.53	19.2	0.35	415	0.988
	80	0.67	13.5	0.30	372	0.982
30	20	0.51	28.4	0.34	614	0.987
	40	0.54	21.6	0.31	569	0.987
	60	0.56	19.8	0.30	498	0.986
	80	0.61	14.2	0.29	380	0.977